Synthesis, Spectroscopic (FT-IR, FT-Raman), First Order Hyperpolarizability, NBO And Molecular Docking Study Of (E)-3-(1,3-Benzodioxol-5-yl)-N-(4-Fluorophenyl)Prop-2-Enamide

S.Syed Shafi[1], P.Chakkaravarthy[2]
[1, 2] Dept of Chemistry
[1] Thiruvalluvar University, Vellore, Tamil nadu India
[2]Government Thirumagal Mills College Gudiyattam, India

Abstract- *The title compound, (E)-3-(1,3-benzodioxol-5-yl)-N-(4-fluorophenyl)prop-2-enamide(BN4FPP) has been synthesized and characterized by FT-IR and FT-Raman spectral analysis. The molecular structure, fundamental vibrational frequencies, and intensity of the vibrational bands are interpreted with the aid of the structure optimizations and normal coordinate force field calculations based on density functional theory (DFT) method using 6-311++G(d,p) basis set. A complete assignment and analysis of the fundamental vibrational modes of the molecule were carried out. The vibrational studies were interpreted in terms of potential energy distribution. Besides NLO were also calculated and interpreted. To study the biological activity of the investigation molecule, molecular docking was done to identify the hydrogen bond lengths and binding energy with different antimicrobial protein*

I. INTRODUCTION

The synthesis of chalcone enamide derivatives has generated vast interest in organics as well as for medicinal chemistry, agricultural and many other industrial processes [1]. Several chalcone enamide derivatives have proved the efficiency and efficacy in combating various diseases. Particularly, enamide and indol derivatives (E)-3-(1,3-benzodioxol-5-yl)-N-(4-fluorophenyl)prop-2-enamide(BN4FPP) wide variety of biological activities such as antifungal, antibacterial, antituberculosis, antitumor, hypoglycemic, anti-inflammatory,analgesic and antipyretic activities [2-3]. Its chemical formula is C16H12FNO3. To our knowledge, Literature survey reveals that the DFT/B3LYP frequency calculations of BN4FPP have not been carried out so far. In this present work, we report the synthesis and comprehensive spectroscopic investigation of BN4FPP using B3LYP/6-311++G(d,p) level of the theory. The experimental spectral data (FT-TR, and FT-Raman) of the BN4FPP is compared by means of the theoretical spectral data obtained by DFT/B3LYP method 6-311++G(d,p) basis set.

Synthesis

A mixture of equimolar (0.01) concentrations of 1.35 g of finely powdered N-phenylacetamide and 1.5 g 2H benzodioxole-4-carbaldehyde we amount of ethanol (30ml) taken in a round bottom flask. Sufficient 2N KOH solution was added to the above solution and continuous stirring for 4 hrs in ice-cold condition till yellow precipitate was formed. This was then neutralized 2N HCl and dilutes with water and left overnight. The precipitate chalcones were filtered and washed with water and recrystallized from ethanol.

Experimental

The FT-IR spectrum of the synthesis compound E)-3-(1,3-benzodioxol-5-yl)-N-(4-fluorophenyl)prop-2-enamide (BN4FPP) was recorded in the region 4000-450 cm-1 in evacuation mode using a KBr pellet technique with 1.0 cm-1 resolution on a PERKIN ELMER FT-IR spectrophotometer. The FT-Raman spectrum of the BN4FPP compound was recorded in the region 4000-100 cm-1 in a pure mode using Nd: YAG Laser of 100 mW with 2 cm-1 resolution on a BRUCKER RFS 27 at SAIF, IIT, Chennai, India.

II. COMPUTATIONAL DETAILS

The optimized structure of the title compound, corresponding energy, and vibrational harmonic frequencies were calculated by using DFT (B3LYP) / 6-311++G(d, P) basis set using GAUSSIAN 03W program package [4]. Without any constraint on the geometry the energy of the title molecule was minimized, whole intramolecular forces were brought to be zero. The geometry was optimized at B3LYP level by using 6-311++G(d,p) basis set. The frequency

calculation delivered the fundamental vibrational frequencies, optimized geometrical parameters, energy, thermodynamical data such as entropy, enthalpy, and heat capacity. Also, IR and Raman spectra were stimulated. Mulliken population analysis determined the distribution of electrons into the molecular orbitals. The symmetries of the vibrational modes were determined by using the standard procedure [5] of decomposing the traces of the symmetry operation into the irreducible representations. By combining the result of the Gaussview program [6] with symmetry considerations, vibrational frequency assignments were performed. Calculation of potential energy distribution (PED) and the prediction of IR and Raman intensities were done with VEDA 4 program [7]. The NBO analysis and MEP calculations were performed on the title molecule. NBO give clear evidence stabilization originating from hyperconjugation of various intramolecular interactions [8-10]. The Mulliken populations were reported. Furthermore, various non-linear optical properties of BN4FPP such as dipole moment, the anisotropy of polarizability and first-order hyper polarizability were also computed on theoretical computations.

2.1Prediction of Raman intensities

The Raman activities (S_i) calculated by Gaussian 03 program have been suitably adjusted by the scaling procedure with MOLVIB and subsequently converted to relative Raman intensities (I_i) using the following relationship derived from the basic theory of Raman scattering [11].

$$I_i = \frac{f(\upsilon_0-\upsilon_i)^4 S_i}{\upsilon_i [1 - \exp (hc\upsilon i/k_b T)]},$$

Where v_o is the exciting frequency (in cm), $v_i$is the vibrational wave number of the *ith* normal mode, h,c, and k are universal constants, and the f is the suitably chosen common scaling factor for all the peak intensities. For the plots of simulated IR and Raman spectra, pure Lorentzian band shapes are used with a full width at half maximum of 10 cm^{-1} [12].

III. RESULTS AND DISCUSSION

3.1Geometrical structure

The optimized structure parameters of BN4FPP was calculated at B3LYP levels with the 6-311++G(d,p) basis set and are listed in Table 1. in accordance with the atom numbering scheme as obtained from CHEMCRAFT software Fig 1.The table 1 of comparison for the experimental XRD data available from the literature [13] and the calculated bond angle and bond length for BN4FPP is given in Table1.While comparing these values we can see that both are nearly the same, in case of any slight deviation is due to the fact that the theoretical calculations belong to the molecule in the gaseous phase and the experimental results belong to the solid phase [14-15]. In spite of the slight difference in the calculated geometrical parameters, they represent a good approximation and they form the base for calculating other parameters such as vibrational frequencies and thermodynamic properties [16-18].This molecule has sixteen C-C bond lengths, eleven C-H bond lengths, three O-C, two (C–O, N-C) bond lengths and one (N–H) bond lengths respectively. The highest bond length was calculated for C9 – C12, C1 – C2 found to be 1.760 and 1.486 Å. The calculated bond length values for C-C and C-H in the benzene ring vary from 1.486- 1.344 Å and 1.097-1.079 Å by B3LYP/6-311G(d,p) basis set. The C-C bond lengths are higher than the C-H bond lengths. The important reasons for the same charges are repulsive and opposite charges are attractive.

3.2Vibrational Assignments

The experimental FT-IR and FT-Raman spectra for (E)-3-(1,3-benzodioxol-5-yl)-N-(4-fluorophenyl)prop-2-enamide(BN4FPP) are shown in Fig 2 and Fig 3. The vibrational frequencies calculated at B3LYP/6-311++G(d,p) levels were scaled to a factor 0.9641. The vibrational frequencies along with the approximate description of each normal mode of vibration obtained using the basis set B3LYP/6-311++G(d,p) are given in Table 2. The relative intensities were obtained by dividing the computed value by the intensity of the strongest line. Computed intensities and the observed values show intermediate deviation since the computed wave numbers correspond to the isolated molecular state whereas the observed wave numbers corresponding to the solid state spectra. ChemCraft, which is a graphical interface, was used to assign the calculated harmonic wave numbers using displacement vectors to identify the motion of modes.The predicted vibrational wave numbers and the experimental data are well in agreement with each other.

3.2.1C-H vibrations

In the aromatic compounds, the C-H stretching wavenumbers appear in the range 3000-3100 cm-1 which are the characteristic region for the ready identification of C-H stretching vibrations [19]. The C-H stretching and bending regions are of the most difficult regions to interpret in infrared spectra. The nature and position of the substituent cannot affect these vibrations. Most of the aromatic compounds have almost four infrared peaks in the region 3080-3010 cm-1 due

to ring C-H stretching bands [20]. In this present study, the C-H stretching vibrations are observed at 3117, 3076, 3069, 3067, 3059, 3032 and 3002 cm-1 by B3LYP/6-311++G(d,P) method show good agreements with experimental vibrations. The bands observed in the recorded FT-IR spectrum 3127(s), 3074(m), 2998(m) cm-1 and with the FT-Raman spectrum bands at 3118(s), 3069(vs), 3060(vs), 3045(s), 3031(s) cm-1. The PED corresponding to this pure mode of title molecule contributed 98, 96, 90, 96, 88, 97 and 99% are shown in Table.2

3.2.2 C-C ring vibrations

The C-C stretching vibrations are expected in the range from 1650 to 1100 cm-1 which are not significantly influenced by the nature of the substituent [21]. The C-C stretching vibrations of the BN4FPP compound were observed from1625 to 910 cm-1. In this present study, the C-C stretching vibrations are found at 1606(vs), 1537(vs), 1489(vs), 1449(vs), 1393(vs), 1370(s), 1314(vs), 1260(vs), 1090(s), 928(s) cm-1 in FT-IR and 1622(s), 1592(vs), 1540(s), 1493(s), 1448(s), 1393(m), 1360(s), 1257(s), 1237(s), 1180(s), 1119(s) cm-1 in FT-Raman respectively.
Fig 1 the scheme of the synthesis of BN4FPP

3.2.3 C-C ring vibrations

The C-C stretching vibrations are expected in the range from 1650 to 1100 cm-1 which are not significantly influenced by the nature of the substituents [21]. The C-C stretching vibrations ofthe 3B5NCE compound were observed from1625 to 910 cm-1. In this present study, the C-C stretching vibrations are found at 1606(vs), 1537(vs), 1489(vs), 1449(vs), 1393(vs), 1370(s), 1314(vs), 1260(vs), 1090(s), 928(s) cm-1 in FT-IR and 1622(s), 1592(vs), 1540(s), 1493(s), 1448(s), 1393(m), 1360(s), 1257(s), 1237(s), 1180(s), 1119(s) cm-1 in FT-Raman respectively.

The theoretical wavenumbers at 1614, 1581, 1561, 1482, 1460,1412, 1368, 1335, 1270, 1254, 1244, 1187, 1118, 1094 and 911 cm-1 are assigned as C-C stretching vibrations with PED contribution of 59, 64, 58, 22, 23, 29, 45, 54, 28, 23, 25, 46, 39, 27 and 57% respectively.

3.2.4 C-O vibration

The C-O stretching vibration occurs at 1627 (vs) cm−1 in FTIR and 1626 cm−1 in solid FT-Raman [22]. Normally, the C–O stretching vibrations occur in the region 1260-1000 cm-1 [17]. The C-C stretching vibrations of the BN4FPP compound were observed from1660 to 1010 cm-1. In this present study, the C-C stretching vibrations are found at 1681(vs), 1038(vs) cm-1 in FT-IR and 1663(vs), 1010(vs) cm-1 in FT-Raman. The theoretical wavenumbers at 1656, 1016 cm-1 are assigned as CC stretching vibrations with PED contributions of 72, 76%.

IV. NLO PROPERTIES

Non-linear optical (NLO) effects arise from the interactions of electromagnetic fields in various media to produce new fields altered in phase, frequency, amplitude or other propagation characteristics from the incident fields[23-25]. Organic molecules that exhibit extended p conjugation, in particular, show enhanced second-order NLO properties. [26-27].

The first hyperpolarizability(β) of this novel molecular system and the related properties (μ,α, β_0) of LAO are calculated using the B3LYP/6-311++G(d,p) basis set, based on the finite field advance. In the presence of a useful electric field, the energy of a system is a function of the electric field. The first hyperpolarizability is a third-rank tensor that can be described by a 3 x 3 x 3 matrix. The 27 components of the 3D matrix can be reduced to 10 components due to the Klein man symmetry [28]. It can be given in the lower tetrahedral. The components are defined as the coefficients in the Taylor series expansion of the energy in the external electric field. When the external electric field is weak and homogenous, this expansion becomes:

$$E = E^{O} - \mu\alpha F\alpha - 1/2\alpha\alpha\beta F\alpha F\beta - 1/6\beta\alpha\beta\gamma F\alpha F\beta F\gamma + \ldots..$$

The total static dipole moment is

$$\mu = (\mu^2_x + \mu^2_y + \mu^2_z)^{1/2}$$

The isotropic polarizability is

$$\alpha_0 = \alpha_{xx} + \alpha_{yy} + \alpha_{zz}/3$$

The polarizability anisotropy invariant is

$$\alpha = 2^{1/2}[(\alpha_{xx} - \alpha_{yy})^2 + (\alpha_{yy} - \alpha_{zz})^2 + (\alpha_{zz} - \alpha_{xx})^2 + 6\,\alpha^2_{xx}]^{1/2}$$

and the average hyperpolarizability is

$$\beta = (\beta^2_x + \beta^2_y + \beta^2_z)^{1/2}$$
$$\beta_x = \beta_{xxx} + \beta_{xyy} + \beta_{xzz}$$
$$\beta_y = \beta_{yyy} + \beta_{xxy} + \beta_{yzz}$$
$$\beta_z = \beta_{zzz} + \beta_{xxy} + \beta_{yyz}$$

Where E^o is the energy of the unperturbed molecules, F is the field at the origin and are the components of dipole moment, polarizability, and first-order hyperpolarizabilities,

respectively. The total static dipole moment (μ), polarizability (α) and the first order hyperpolarizability(β), using the x,y,z components are defined as follows. The calculated hyperpolarizability values of BN4FPP are listed in Table 3 In our present study, the first order hyper-polarizabilities, polarizabilities and dipole moment of BN4FPP were calculated and values are listed in Tabl.3. The calculated first hyperpolarizability of the title molecule is 8.3198 $x10^{-26}$esu.The calculated values of μ, α for the title compound are 2.4681 D, $3.7074x10^{-23}$ esu which are greater than those of urea (μ, α of urea are 1.3732 D, $0.3728 x10^{-30}$ esu obtained by 3LYP/6-311++G(d,p) method Urea is one of the prototypical molecules utilized investigating of the NLO properties of compound. For this reason, urea was used often as a threshold value for comparative purpose. The first-order hyperpolarizability of title molecule is 26 times magnitude of urea. The results indicate that the title molecule is a good candidate for NLO material.

V. NBO ANALYSIS

NBO analysis transforms molecular orbital wave functions into one-center (lone pair) and two-center (bond) representations [29]. The advantage of NBO analysis is that they provide insight into the interactions between various parts of the molecule [30]. The bond-anti bond and lone-pair-anti bond interactions can be calculated by two difference procedures following the NBO method [31]. The first one is an indirect procedure as suggested by Weinhold, which involves comparison of barrier energies calculated with and without the Fock matrix element (F_{ij}) [32]. The second procedure involves the estimations of all possible interactions between "filled" (donor) Lewis type NBO s and "empty" (acceptor) non-Lewis NBOs, by considering their energetic importance using second-order perturbation theory. Since these interactions lead to the donation of occupancy from the localized NBOs of the idealized Lewis structure into the empty non-Lewis orbitals, they are referred to as "delocalization" corrections to the zeroth-order natural Lewis structure. For each donor, NBO (i) and acceptor (j), the stabilization energy E(2) associated with delocalization i –> j is represented as:

$$E(2) = \Delta E_{ij} = q_i (F_{ij})^2 / (\varepsilon_j - \varepsilon_i)$$

Where q_i is the donor orbital occupancy, F_{ij} is the off-diagonal and ε_j,ε_i are diagonal elements specifying the respective orbital energies of the NBO Fock matrix.

NBO analysis has been performed on the molecule at the B3LYP/6-311+ +G (d,p) level in order to elucidate the intra molecular, rehybridization and de-localization of electron density within the molecule. The strong intramolecular hyper conjugative interaction of the σ and π electrons of C-C to the antibonding C-C bond in the ring leads to stabilization of some part of the ring as evident from Table 4. The strong intramolecular hyper conjugative interaction of the σ and π electrons of C-C to the anti C-CC bond of the ring leads to stabilization and evidence of some part of ring values are listed in Table.4. The strong intramolecular hyperconjugative interaction of σ (C6-C7) distributes to σ * (C6-C11, C7-C8, and C9-C10 of the ring. On the other hand, side the π C6- C7 in the ring conjugate to the anti-bonding orbital of π*(C8-C9) and π*(C10-C11) which leads to strong delocalization of 28.620 and 19.91 kJ/mol respectively. Some important second-order perturbation energies and molecular orbital interactions investigated from the NBO calculation between Lewis and non-Lewis orbital with Oxygen and nitrogen lone pairs. The very significant interaction between them was the electron donation of LP(2) O4, LP(1) N5, LP(1) Cl12, LP (2) O13 and O15 to the neighbouring antibonding acceptor σ*(C1-C2), σ*(C1-N5), σ*(C11-H28), π*(C1-O4), π*(C20- C21), σ*(N1-C3), π*(C17-C21) and π*(C16-C18) of the 3B5NCE energy by 14.75, 16.07, 43.12, 86.12, 16.71, 46.20 and 91.19 kJ/mol.

VI. MOLECULAR ELECTROSTATIC POTENTIALS

Molecular electrostatic potential (MEP) simultaneously displays molecular shape, size, and electrostatic potential in terms of colour grading. MEPs map has been found to be a very helpful tool in the analysis of the correlation amid molecular structures with its physiochemical property relationship, including biomolecules and drugs [33]. MEPs map and contour plot of the (E)-3-(1,3-benzodioxol-5-yl)-N-(4-fluorophenyl)prop-2-enamide(BN4FPP) generated at the optimized geometry of the title molecule using GaussView 5.0 program is shown in Fig.4.. The various values of the electrostatic potential are represented by various colors; red represented the regions of the most negative electrostatic potential, blue represents the regions of the most positive electrostatic potential and green presents the region of zero potential. The potential increases in the order red < orange < yellow < green < cyan < blue. It can be seen that the negative regions are mainly over the F1,N5,O2,O3 and O4 atoms. Negative (red color) and positive (blue) regions of electrostatic potential are associated with electrophilic and nucleophilic reactivity. The majority of light green region MEP surface resemble a potential halfway between two extremes red and dark blue color. The negative molecular electrostatic potential resembles to an attraction of the proton by the evaluate electron density in the molecule (shades of red), the positive electrostatic potential corresponds to the repulsion of the protons by the atomic nuclei (shades of blue).

According to these calculated results, the MEP map illustrates that the negative potential sites are on oxygen nitrogen and fluorine atoms and the positive potential sites as well are around the hydrogen atoms. These active sites found to be clear evidence of biological activity in the title compound.

VII. HOMO-LUMO ANALYSIS

The highest occupied molecular orbital (HOMO) and the lowest unoccupied molecular orbital (LUMO) are very important parameters for quantum chemistry [34]. We can determine the way the molecule interacts with other species; hence, they are called the frontier orbitals. Both the highest occupied molecular orbital (HOMO) and the lowest unoccupied molecular orbital (LUMO) are the main orbitals that take part in chemical stability. The HOMO represents the ability to donate an electron, LUMO as an electron acceptor obtains electron. This electronic absorption corresponds to the transition from the ground to the first excited state and is mainly described by one electron excitation from the highestoccupied molecular orbital (HOMO) to the lowest unoccupied molecular orbital (LUMO). Owing to the interaction between HOMO and LUMO orbitals of a structure, transition of π^* - π^* type is observed with regards to the molecular orbital theory [34]. Therefore, while the energy of the HOMO is directly related to the ionization potential, LUMO energy is directly related to the electron affinity. Energy difference between HOMO and LUMO orbital is called as energy gap that is an important stability for structures [35]. The HOMO is spread totally only on Ring1 and mostly on Iodine, to a less extent on chlorine and to a smaller extent on oxygen. The excitation of electron from HOMO to LUMO implies an electron density transfer mostly from the iodine and also from Ring1 to Ring2 and C=O. Evidently Ring2 now has an overall electron density distribution and also C=O. A overlap is also observed on both the rings through inter ring. The 3D plots of highest occupied molecular orbitals (HOMOs) and lowest unoccupied molecular orbitals (LUMOs) is shown in Fig.5.Table.5

VIII. MOLECULAR DOCKING STUDY

Molecular docking study Auto Dock suite 4.2.6 is a recently been used as a convenient tool to get insights into the molecular mechanism of protein-ligand interactions bind to a receptor of the known three-dimensional structure. With the aim to investigate the binding mode, a molecular modeling study was performed using AutoDock Tools for docking [37]. BN4FPP was selected to be docked into the active site of two BN4FPP o receptors 4y95and 3QNJ of antimicrobial proteins which were downloaded from RCSB protein data bank (http://www.rcsb.org/pdb/home/home.do) [38]. The ligand was docked into the functional sites of the respective proteins individually and the docking energy was examined to achieve a minimum value. AutoDock results indicate the binding position and bound conformation of the peptide, together with a rough estimate of its interaction. Docked conformation which had the lowest binding energy was chosen to investigate the mode of binding. The molecular docking binding energies (kcal/mol) and inhibition constants (μm) were also obtained and listed in Table 4. Among them, 4Y95 exhibited the lowest free energy at -8013 kcal/mol and most docked inhibitors interacted with the ligand within the 4Y95 binding site. They exhibited up to two N H …O hydrogen bonds involving ASN 484 and CYS 481 with RMSD being 44.53 Å. The docking simulation shows the binding mode of the BN4FPP into 4Y95. The BN4FPP ligand interacts with different receptors are shown in Figs.6.7.

IX. CONCLUSION

In the present work, we have thoroughly analyzed spectroscopic (FT-IR, FT-Raman), NLO and NBO analysis of BN4FPP molecule with B3LYP/6-311++G(d,p) method. The structural parameters, vibrational frequencies, infrared intensities and Raman activities calculated by B3LYP/6-311++G(d,p) method agree very well with experimental results. The complete vibrational assignments of wave numbers are made on the basis of potential energy distribution (PED). The nonlinear optical properties are also addressed theoretically. The first order hyperpolarizability of the title compound is twenty six times greater than the value of urea. Furthermore, antimicrobial studies of the title molecule show that a molecule is an attractive object for the future studies of biological activity.

REFERENCES

[1] O.A. Luzina, D.N. Sokolov, M.A. Pokrovskii, A.G. Pokrovskii, O. B. Bekker, V.N. Danilenko N.F. Salakhutdinov, synthesis and biological activity of usnic acid Enamine derivatives, Chemistry of Natural Compounds, 51 (2015) 646-651.

[2] R. Matsubara, S. Kobayashi, Enamides and Enecarbamates as Nucleophiles in stereoselective C-C and C-N Bond-Forming Reactions,Acc.chem,RES,41 (2008) 292-301.

[3] D.R. Carbery, Enamides: valuable organic substrates, Org. Biomol. Chem. 6 (2008) 3455-3460

[4] Gaussion 03 Program, Gaussian Inc., Wallingford, CT, 2004.

[5] P. Hohenberg, W. Kohn, Phys. Rev. 136 (1964) B864–B871.

[6] A. Frisch, A.B. Neilson, A.J. Holder, Gauss View Users Manual, Gaussian Inc.,Pittsburgh, PA, 2000.
[7] M.H. Jamroz, Vibrational Energy Distribution Analysis: VEDA 4 Program, Warasaw, Poland, 2004.
[8] X.-H. Li, R.-Z. Zhang, X.-Z. Zhang, Struct. Chem. 20 (2009) 1049–1054.
[9] J. Chocholousova, V. VladiminSpirko, P. Hobza, Phys. Chem. 6 (2004) 37–41.
[10] A.E. Reed, L.A. Curtiss, F. Weinhold, Chem. Rev. 88 (1988) 899–926.
[11] G. Keresztury, S. Holly, J. Varga,, G. Besenyei, A.Y. Yang, J.R. Durig, SpectrochimActa A
49 (1993), pp: 2007-2026.
[12] G. Keresztury, in: J.M. Chalmers, P.R. Griffth (Eds.), Raman Spectroscopy: Theory in
Handbook of vibrational spectroscopy, vol 1, John Wiley & Sons Ltd., New York, 2002
[13] A.M. Asiri, M. Akkurt, S. A. Khan, I. Ullah Khan and M.N. Arshad, "(E)-2-Cyano-3-[4-(dimethylamino) phenyl]- N -phenylprop-2-enamide", Acta Cryst.(2009). E65, 1303.
[14] H.B. Schlegel, J. Comput. Chem. 3 (1982) 214–218.
[15] G. Socrates, Infrared and Raman Characteristics Group Frequencies, Tables and Charts,
third ed., Wiley, Chichester, 2001.
[16] R. Shanmugam, D. Sathyanarayanan, Spectrochim. Acta A 40 (1984) 757–761.
[17] P. Vandenabeela, L. Moens, H.G.M. Edwards, R. Dams, J. Raman Spectrosc. (2000) 509–566.
[18] P.J. Trotter, Appl. Spectrosc. 31 (1977) 30–38.
[19] N. Swarnalatha, S.Gunasekaran, S. Muthu, M. Nagarajan, Molecular structure analysis andspectroscopic characterization of 9-methoxy-2Hfuro[3,2-g]chromen-2-one with experimental (FT-IRand FT-Raman) techniques and quantum chemical calculations, spectrochim. Acta part A 137 (2015) 721-729
[20] L.G. Wade (Ed), Advanced Organic Chemistry, 4th ed., Wiley, New York, 1992. p.723.
[21] N. Sundaraganesan, S.Illakiamani, C. Meganathan, B.D.Joshua, Vibrational spectroscopy investigation using ab initio and density functional theory analysis on the structure of 3-aminobenzotrifluoride, Spectrochim. Acta A 67 (2007) 214-224.
[22] T. Gnanasambandan, S. Gunasekaran, and S. Seshadri, vibrational spectroscopic investigation on propylthiouracil, International Journal of Recent Scientific Research, 3 (2012) 590 -597
[23] M. Nakano, H. Fujita, M. Takahata, K. Yamaguchi, J. Am. Chem. Soc. 124 (2002) 9648–9655.
[24] V.M. Geskin, C. Lambert, J.L. Bredas, J. Am. Chem. Soc. 125 (2003) 15651–15658.
[25] D. Sajan, H. Joe, V.S. Jayakumar, J. Zaleski, J. Mol. Struct. 785 (2006) 43–53.
[26] J. Indira, P.P. Karat, B.K.Sarojini , J. Crystal Growth 242 (2002) 209-214
[27] B.K. Sarojini, B. Narayana, B.V. Ashalatha, J. Indira, K.G. Lobo, J. Crystal Growth 295 (2006) 54–59
[28] S.T. Kanchana, K.M. Nalin de Silva, J. Mol. Struct. (Theochem) 617 (2002) 169–175.
[29] J. Karpagam, N. Sundaraganesan, S. Sebastian, S. Manoharan, M. Kurt, J. Raman Spectrosc.41 (2010) 53–62.
[30] A.E. Reed, F.J. Weinhold, Chem. Phys. 78 (1993) 4066–4073.
[31] L. Goodman, H. Gu, J. Chem. Phys. 109 (1998) 72–78.
[32] A.E. Reed, F. Wienhold, Isr. J. Chem. 31 (1991) 277–285.
[33] S.K. Pathak, R. Srivastava, A.K. sachan, O. Prasad, L. Sinha, A.M. Asiri, M. Karabacak,Experimental (FT-IR, FT-Raman, UV and NMR) and quantum chemical studies on molecular structure, spectroscopic analysis, NLO, NBO and reactivity descriptors of 3,5- Difluoroanilin, Spectrochim.Acta A 135 (2015) 283-295
[34] S. Sudha, N. Sundaraganesan, M. Kurt, M. Cinar, M. Karabacak, FT-IR and FTRaman spectra, vibrational assignments, NBO analysis and DFT calculations of 2-amino-4-chlorobenzonitrile, J. Mol. Struct. 985 (2011) 148-156.
[35] K. Fukui, Theory of Orientation and Stereoselection, vol. 218, Springer-Verlag,Berlin, 1975-1987, p. 747. See also: Fukui, K. Science.
[36] L. Ding, H. Ying, Y. Zhou, T. Lei, J. Pei, Polycyclic imide derivatives: synthesis and effective tuning of lowest unoccupied molecular orbital levels through molecular engineering, Org. Lett. 12 (2010) 5522-5525.
[37] N.T. Abdel-Ghani , M.F.A. El-Ghar, A.M. Mansour,Novel Ni(II) and Zn(II) complexes coordinated by 2-arylaminomethyl-1H-benzimidazole: Molecular structures, spectral, DFT studies and evaluation of biological activity, Spectrochimica Acta A 104 (2013) 134-142.
[38] A.R. Katritzky, L. Mu, V.S. Lobanov, M. Karelson, Correlation of Boiling Points with Molecular Structure. 1. A Training Set of 298 Diverse Organics and a Test Set of 9 Simple Inorganics, J. Phys. Chem. 100 (1996) 10400-10407.

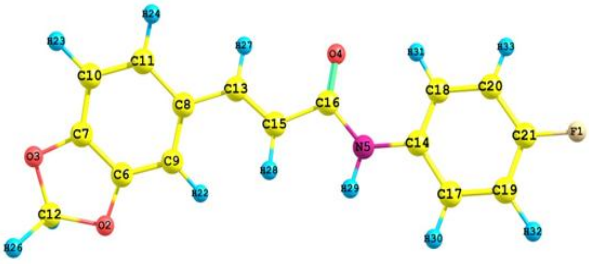

Fig 1 Optimized structure with atoms numbering of BN4FPP

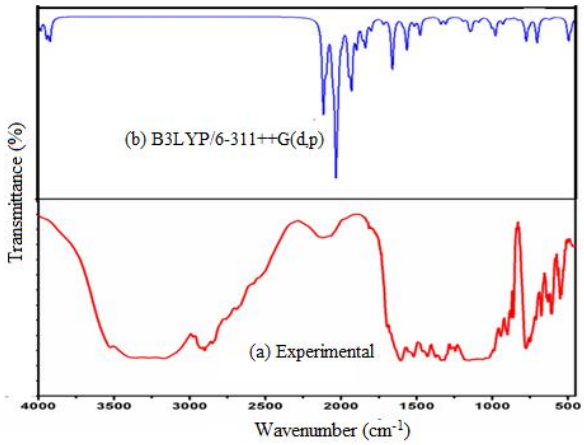

Fig.2. FT-IR spectra of BN4FPP: (a) Experimental, (b) B3LYP/6-311++G(d,p).

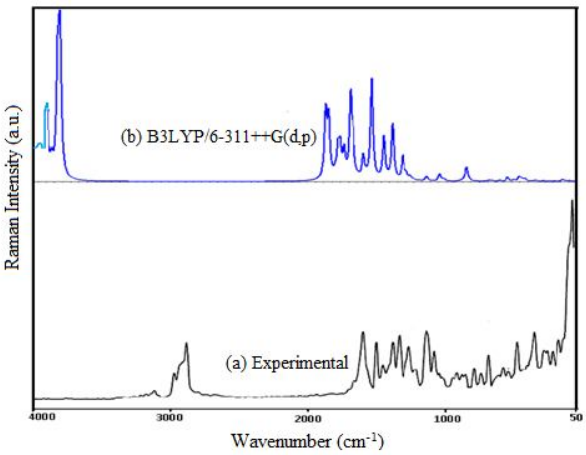

Fig.3. FT-Raman spectra of BN4FPP: (a) Experimental, (b) B3LYP/6-311++G(d,p).

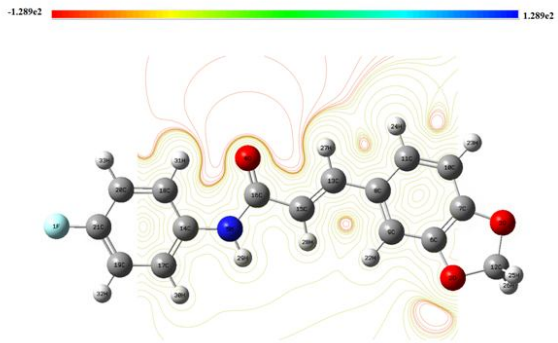

Fig. 4. The contour map of electrostatic potential of the total density of of BN4FPP

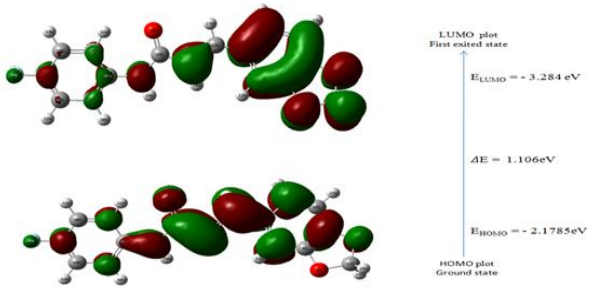

Fig.5. Atomic orbital HOMO – LUMO composition of the frontier molecular orbital for BN4FPP

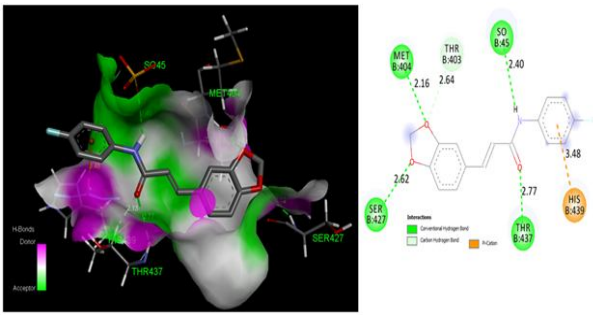

Fig.6. Docking and Hydrogen bond interactions BN4FPP with chain A of 3QNJ protein structure.

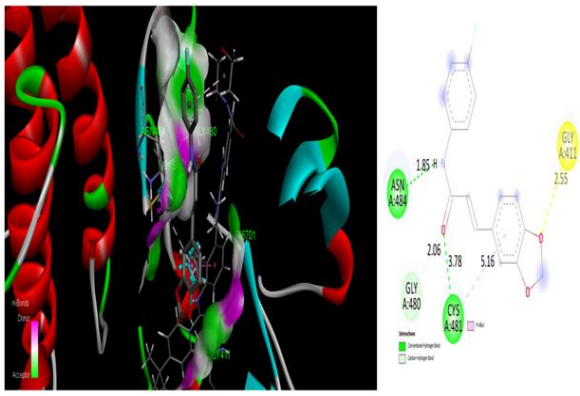

Fig. 7. Docking and Hydrogen bond interactions BN4FPP with chain A of 4Y95 protein structure

Table.1 Optimized parameters of (E)-3-(1,3-benzodioxol-5-yl)-N-(4-fluorophenyl)prop-2-enamide(BN4FPP) obtain by B3LYP/6-311++G(d,p) basis set.

Parameter	B3LYP/ 6-311++ G(d,p)	Parameter	B3LYP/ 6-311++ G(d,p)	Parameter	B3LYP/ 6-311++ G(d,p)
Bond Length (A)		Bond Angle (0)		Bond Angle (0)	
C1-C2	1.493	1.486	C2-C1-O4	121.2	120.6
C1-O4	1.216	1.223	C2-C1-N5	116.3	115.9
C1-N5	1.363	1.382	C1-C2-C3	125.7	126.2
C2-C3	1.349	1.344	C1-C2-H22	114	112.1
C2-H22	0.96	1.084	O4-C1-N5	124	123.5
C3-C19	1.45	1.465	C1-N5-C6	128.4	128.9
C3-H23	0.96	1.089	C1-N5-H24	116.3	115.8
N5-C6	1.422	1.408	C3-C2-H22	120	121.5
N5-H24	0.86	1.008	C2-C3-C19	125.7	127.6
C6-C7	1.407	1.403	C2-C3-H23	119	118.5
C6-C11	1.407	1.402	C19-C3-H23	114	113.9
C7-C8	1.39	1.389	C3-C19-C18	117.7	117.8
C7-H25	0.96	1.086	C3-C19-C20	122.4	122.8
C8-C9	1.39	1.391	C6-N5-H24	116	115
C8-H26	0.96	1.082	N5-C6-C7	116.3	117.4
C9-C10	1.39	1.39	N5-C6-C11	124.7	123.6
C9-Cl12	1.493	1.76	C7-C6-C11	119	119
C10-C11	1.39	1.393	C6-C7-C8	120.5	121
C10-H27	0.96	1.083	C6-C7-H25	120	119.9
C11-H28	0.96	1.079	C6-C11-C10	119.9	119.8
O13-C14	1.296	1.436	C6-C11-H28	120	119.7
O13-C17	1.296	1.37	C8-C7-H25	119	119.1
C14-O15	1.216	1.433	C7-C8-C9	119	119.2
C14-H29	0.96	1.089	C7-C8-H26	120	120.4
C14-H30	0.96	1.097	C9-C8-H26	120	120.4
O15-C16	1.216	1.374	C8-C9-C10	120.6	120.5
C16-C17	1.393	1.39	C8-C9-Cl12	119.4	119.6
C16-C18	1.375	1.375	C10-C9-Cl12	119.9	119.8
C17-C21	1.385	1.381	C9-C10-C11	120.6	120.3
C18-C19	1.407	1.416	C9-C10-H27	120	120
C18-H31	0.96	1.083	C11-C10-H27	120	119.7
C19-C20	1.407	1.404	C10-C11-H28	120	120.4
C20-C21	1.397	1.398	C14-O13-C17	112	105.2
C20-H32	0.96	1.082	O13-C14-O15	107.8	107.2
C21-H33	0.96	1.082	O13-C14-H29	109	109.4
			O13-C14-H30	110	109.2
			O13-C17-C16	109	109.7
			O13-C17-C21	121.2	128.7
			O15-C14-H29	109	109.5
			O15-C14-H30	110	109.4
			C14-O15-C16	105	105.2
			H29-C14-H30	110	111.9
			O15-C16-C17	109	109.5
			O15-C16-C18	121.2	128.5
			C17-C16-C18	121.9	122
			C16-C17-C21	121.9	121.9
			C16-C18-C19	118.2	117.9
			C16-C18-H31	120	120.9
			C17-C21-C20	117.7	117.1
			C17-C21-H33	120	121.3

C19-C18-H31	120	121.2
C18-C19-C20	119.9	119.3
C19-C20-C21	121.9	122.1
C19-C20-H32	120	119.6
C21-C20-H32	119	118.3
C20-C21-H33	120	121.6

aTken from Ref[13]

Table 2 Calculated vibrational frequencies (cm-1) assignments of BN4FPP based on B3LYP/6-311++G(d,p) basis set.

Sl. No	**Frequency (cm^{-1})**				**Intensity**		
	Experimental		Theoretical		IR	Raman	**[d]Assignments (PED≥10%)**
	FT-IR	FT-Raman	Unscaled	[a]Scaled	[b]Relative	[c]Relative	
93	-	-	3624	3483	3	5	γNH(100)
92	3127(s)	3118(s)	3243	3117	2	3	γCH(98)
91	-	-	3207	3082	1	7	γCH(92)
90	3074(m)	-	3201	3076	0	5	γCH(96)
89	-	-	3197	3072	0	4	γCH(98)
88	-	3069(vs)	3193	3069	0	1	γCH(90)
87	-	3060(vs)	3191	3067	0	2	γCH(96)
86	-	3045(s)	3183	3059	2	2	γCH(-88)
85	-	3031(s)	3155	3032	3	2	γCH(97)
84	-	-	3125	3003	6	9	γCH(93)
83	2998(m)	-	3124	3002	4	2	γCH(99)
82	-	-	3012	2894	27	14	γCH(93)
81	1681(vs)	1663(vs)	1724	1656	68	79	γOC(72)
80	1606(vs)	1622(s)	1679	1614	6	21	γCC(59)
79	-	1592(vs)	1645	1581	12	100	γCC(64)
78	-	-	1639	1575	2	8	γCC(60)
77	-	-	1635	1571	4	54	γCC(-52)+βHCC(-17)
76	1537(vs)	1540(s)	1624	1561	15	3	γCC(58)+βHNC(-14)+βHCC(12)
75	1489(vs)	1493(s)	1542	1482	100	22	γCC(-11)+βHNC(-43)

74	-	-	1540	1480	22	5	βHCH(79)
73	-	-	1522	1463	28	2	βHCC(41)
72	1449(vs)	1448(s)	1520	1460	69	2	βHCC(-42)+γCC(13)
71	1393(vs)	1393(m)	1470	1412	8	2	βHCC(27)+γCC(29)
70	-	1372(s)	1427	1372	0	2	τHCOC(77)
69	1370	1360(s)	1424	1368	20	3	βHCC(-32)+γCC(-45)
68	1314(vs)	-	1389	1335	30	29	γCC(-54)+βHCC(-12)
67	1291(vs)	1293(vs)	1345	1292	3	4	βHCC(57)+γCC(-10)
66	-	-	1332	1280	34	17	γCC(-42)+βHCC(24)
65	1260(vs)	-	1321	1270	2	2	γCC(28)+βHCC(49)
64	-	1257(s)	1305	1254	18	20	βHCC(25)+γCC(-13)
63	-	1237(s)	1294	1244	32	14	βHCC(-42)+γCC(-11)
62	-	-	1275	1225	16	5	γCC(30)+βHCC(15)
61	-	-	1261	1212	9	22	γCC(58)
60	-	1180(s)	1236	1187	93	14	γCC(-46)+βHCC(11)
59	1170(m)	1171(s)	1219	1172	9	7	βHCC(59)
58	-	-	1201	1155	0	2	βHCC(59)
57	-	-	1200	1153	9	19	βHCC(-33)
56	-	1119(s)	1163	1118	4	0	βHCC(38)+γCC(39)
55	-	1091(vs)	1142	1097	2	0	βHCO(90)
54	1090(s)	-	1138	1094	3	0	βHCC(-58)+γCC(27)
53	-	-	1110	1067	7	11	βHCC(-11)+γCC(21)
52	-	-	1103	1060	17	1	γFC(-11)+βHCC(-13)+γCC(-56)
51	1038(vs)	1010(vs)	1057	1016	31	0	γOC(76)
50	-	-	1025	985	5	1	βHCC(69)+γCC(-18)
49	968(m)	968(m)	1001	962	9	5	τHCCO(-76)
48	-	-	988	950	1	1	γCC(52)
47	-	-	987	948	0	0	τHNCC(-77)
46	928(s)	-	948	911	0	1	γCC(-57)
45	-	-	944	907	9	1	γOC(69)+τHCCN(-89)

44	-	-	944	907	0	0	τHCCC(-84)
43	-	-	941	905	1	0	τHCCO(69)
42	-	-	895	860	2	3	βHNC(21)+τHCCO(-14)+γCC(28)
41	-	845(s)	873	839	1	2	τHCCO(62)
40	829(s)	821(s)	861	828	6	0	τHCCC(87)
39	-	-	852	819	7	0	βHCC(13)+γCC(56)
38	-	-	830	798	3	1	τHCCC(81)
37	-	-	823	791	6	0	τHCCN(-89)
36	784(m)	785(s)	816	784	5	0	βHCC(42)+γCC(15)
35	751(s)	-	806	774	2	0	βHCC(17)
34	-	719(s)	750	721	3	0	βHCC(55)
33	707(m)	709(vs)	731	702	2	1	τHCCC(58)
32	-	-	730	702	1	0	τHNCC(-80)
31	-	-	720	692	0	0	τHCCC(56)
30	-	-	708	680	0	0	βHCC(19)
29	625(m)	632(s)	658	632	1	1	βHCC(-79)
28	607(m)	-	647	622	1	0	τHCCC(-10)+βCCO(-50)
27	-	-	613	589	0	0	τHCCC(-56)
26	-	-	600	577	1	0	τHNCC(-10)
25	-	-	558	536	4	0	τHNCC(-58)
24	506(m)	-	542	521	9	0	τHNCC(78)
23	-	-	518	498	4	0	γFC(-14)+βHCC(-43)
22	-	-	495	476	2	1	τHCCC(48)+βHCC(19)
21	-	-	431	414	1	0	τHCCC(25)+βHCC(-30)
20	-	-	426	410	1	0	τHCCC(97)
19	-	-	421	405	0	0	βHNC(55)
18	-	381(s)	394	379	2	0	τHCCC(-71)
17	-	355(s)	363	349	1	0	τHNCC(-26)+βHCC(12)
16	-	-	348	335	3	0	τHNCC(54)
15	-	-	332	319	1	0	βCCC(46)

14	-	301(s)	299	288	1	0	βCNC(-49)+τHCCN(-14)+βHCC(-10)
13	-	-	269	259	0	0	τHCCN(63)
12	-	-	251	241	0	0	τHCCN(-66)
11	-	173(s)	202	194	0	0	τCNCC(43)
10	-	-	165	159	0	0	βHNC(43)+τHCCO(-16)
9	-	-	142	136	2	0	βHCC(-14)
8	-	-	135	129	0	0	βHNC(11)+τCNCC(-27)
7	-	-	126	122	2	0	τHCOC(-79)
6	-	-	107	103	1	0	τHCCO(39)
5	-	-	68	65	0	0	τHCCO(-48)+βHCC(12)
4	-	-	47	45	0	0	τHCCC(-48)+τHNCC(10)
3	-	-	31	30	0	0	τHCCO(10)+τHNCC(20)+βHCC(25)
2	-	-	22	21	0	0	τHNCC(-47)
1	-	-	15	14	0	0	τCCCC(57)

[a]γ-stretching, β- inplane bending ,ω- outplane bending, τ-torsion, vs-very strong, s- strong, m-medium, w-weak.
[b]scaling factor : 0.961 for B3LYP/6-311+G(d,p)
[c]Relative absorption intensities normalized with highest peak absorption equal to 100.
[d]Relative Raman intensities normalized to 100.

Table.3 The values of calculated dipole mome (D),polarizability (α0), first order hyperpolarizability (βtot) components of 3B5NCE

Title	Enter Values	Title	Enter Values	Title	Enter Values
βxxx	1652.1517	αxx	417.1405	μx	-2.185
βxxy	1089.3198	αxy	7.6179	μy	-1.1096
βxyy	-136.6774	αyy	208.967	μz	-0.2932
βyyy	84.7987	αxz	4.6006	μ(D)	2.4681
βzxx	166.0636	αyz	3.8657		
βxyz	-19.8863	αzz	124.3771		
βzyy	-5.6903				
βxzz	-25.7611	α (e.s.u)	3.7074x10-23		
βyzz	-2.4566				
βzzz	35.5808	Δα (e.s.u)	11.3850x 10-30		
βtot (a.u)	209.3322244				
βtot (e.s.u)	16.4610X10-30				

Table 4 Second order perturbation theory analysis of Fock matrix in NBO basis for BN4FPP

Donor(i)	Type	ED(e)	Acceptor(j)	Type	ED(e)	E(2)a (kJ/mol)	E(j)–E(i)b (a.u.)	F(i, j)c (a.u.)
C1-C2	σ	1.97224	C1-O4	σ*	0.021	4.05	1.38	0.067
			C1-N5	σ*	0.067	4.55	1.35	0.071
			C2-C3	σ*	0.021	4.85	1.37	0.073
C1-O4	σ	1.98732	C1-C2	σ*	0.041	4.28	1.66	0.076
C1-O4	π	1.95749	C2-C3	π*	0.169	7.91	0.41	0.052
			C11-H28	σ*	0.06	3.93	0.48	0.039
			O15-C16	σ*	0.025	2.36	0.61	0.034
			C16-C18	π*	0.395	3.95	0.2	0.028
C1-N5	σ	1.98004	C9-C10	σ*	0.035	12.66	2.55	0.161
C2-C3	π	1.82051	C1-O4	π*	0.413	29.53	0.3	0.09
C3-H23	σ	1.96754	C2-H22	σ*	0.02	5.03	1.01	0.064
N5-H24	σ	1.97771	C1-O4	σ*	0.021	5.19	1.31	0.074
			C20-C21	σ*	0.015	9.26	1.39	0.101
			C21-H33	σ*	0.018	7.03	1.02	0.076
C6-C7	σ	1.96274	C6-C11	σ*	0.034	10.39	1.78	0.122
			C7-C8	σ*	0.02	6.89	1.76	0.099
			C9-C10	σ*	0.035	8.62	1.74	0.11
C6-C7	π	1.64127	C8-C9	π*	0.419	28.62	0.3	0.084
			C10-C11	π*	0.309	19.91	0.34	0.074
C6-C11	σ	1.95236	N5-C6	σ*	0.035	5.4	1.34	0.076
			N5-H24	σ*	0.041	5.39	1.01	0.066
			C6-C7	σ*	0.03	8.54	1.37	0.097
C7-C8	σ	1.96397	C8-C9	σ*	0.033	6.47	1.37	0.084
C7-H25	σ	1.97561	C11-H28	σ*	0.06	54.82	0.69	0.175
			O15-C16	σ*	0.025	32.63	0.82	0.146
			C16-C18	π*	0.395	32.07	0.41	0.113
C8-C9	π	1.68466	C6-C7	π*	0.432	18.84	0.3	0.07
			C10-C11	π*	0.309	21.01	0.34	0.075
C10-C11	π	1.64955	C6-C7	π*	0.432	27.22	0.27	0.079
			C8-C9	π*	0.419	23.57	0.27	0.073
O13-C14	σ	1.98671	C20-C21	σ*	0.015	12.78	1.67	0.13
			C21-H33	σ*	0.018	12.55	1.3	0.114
C14-H29	σ	1.99096	C9-C10	σ*	0.035	10.89	2.07	0.135
C14-H30	σ	1.99127	C20-C21	σ*	0.015	14.36	1.28	0.121
			C21-H33	σ*	0.018	8.9	0.92	0.081
C16-C17	σ	1.96337	O15-C16	σ*	0.025	20.94	1.05	0.133
			C17-C21	σ*	0.03	14.33	1.36	0.125
C16-C18	π	1.68488	C20-C21	σ*	0.015	8.75	1.02	0.091
			C21-H33	σ*	0.018	6.79	0.65	0.064
C18-H31	σ	1.97589	C18-C19	σ*	0.029	11.87	0.77	0.085
			C20-C21	σ*	0.015	13.01	1.25	0.114
C21-H33	σ	1.9754	C9-C10	σ*	0.035	17.31	0.87	0.11

O4	LP(1)	1.95265	C1-N5	σ*	0.067	4.59	1.24	0.068
			C11-H28	σ*	0.06	22.92	0.73	0.116
O4	LP(2)	1.88183	C1-C2	σ*	0.041	14.75	0.9	0.105
			C1-N5	σ*	0.067	16.07	0.91	0.109
			C11-H28	σ*	0.06	43.12	0.4	0.119
N5	LP(1)	1.61559	C1-O4	π*	0.413	86.12	0.3	0.144
			C2-C3	π*	0.169	0.63	0.31	0.013
			C6-C7	π*	0.432	54.61	0.31	0.118
Cl12	LP(1)	1.99199	C20-C21	σ*	0.015	16.72	1.63	0.148
			C21-H33	σ*	0.018	8.71	1.27	0.094
Cl12	LP(2)	1.97339	C8-C9	σ*	0.033	4.37	0.95	0.058
			C9-C10	σ*	0.035	4.46	0.94	0.058
Cl12	LP(3)	1.93307	C8-C9	π*	0.419	13.02	0.34	0.066
O13	LP(1)	1.94583	C11-H28	σ*	0.06	11.55	0.69	0.08
			O15-C16	σ*	0.025	8.2	0.83	0.074
O13	LP(2)	1.80261	C14-H29	σ*	0.033	5.4	0.69	0.057
			C17-C21	π*	0.417	46.2	0.34	0.119
O15	LP(2)	1.81525	C16-C18	π*	0.395	91.19	0.19	0.125

$E(2)^a$ means energy of hyper conjugative interaction (stabilization energy).
$E(j)–E(i)^b$ Energy difference between donor and acceptor i and j NBO orbitals.
$F(i, j)^c$ is the Fock matrix element between i and j NBO orbitals

Table .5. Calculated energy values of [BN4FPP] by using B3LYP/6-311++G(d,p) method.

Basis set	B3LYP/6-311++G(d,p)
HOMO(eV)	-3.284
LUMO(eV)	-2.178
Ionization potential	3.284
Electron affinity	2.178
Energy gap(eV)	1.106
Electronegativity(χ)	2.731
Chemical potential(μ)	-2.731
Chemical hardness(η)	0.553
Chemical softness(s)	0.904159132
Electrophilicity index(ω)	6.743545208

Table.6 Hydrogen bonding and molecular docking with antimicrobial protein targets

Protein (PDB ID)	Bonded residues	No. of hydrogen bond	Bond distance (Å)	Estimated Inhibition Constant (μm)	Binding energy (kcal/mol)	Reference RMSD (Å)
4Y95	ASN 484	2	1.8	1.1	-8.13	44.54
	CYS 481		3.8			
	SER 427	4	2.6			
3QNJ	MET 404		2.2	74	-5.64	25.09
	S0B45		2.4			
	THR437		4.4			